Inorganic Chemistry
Article

*Inorg. Chem.* **2009**, *48*, 6211–6221 **6211**
DOI: 10.1021/ic900515j

# Octahedral Monodithiolene Complexes of Cobalt(III) and Chromium(III). Spectroscopic and Density Functional Theoretical Characterization of *S,S′*-Coordinated Benzene-1,2-dithiolate(1-) $\pi$ Radicals.

**Carsten Milsmann, Eberhard Bothe, Eckhard Bill, Thomas Weyhermüller, and Karl Wieghardt***

*Max-Planck-Institut für Bioanorganische Chemie, Stiftstrasse 34-36, D-45470 Mülheim an der Ruhr, Germany*

Received March 16, 2009

The reaction of [M(tren)$Cl_2$]Cl (M = Co(III), Cr(III)) with benzene-1,2-dithiol, $H_2$(bdt), and 3,6-bis(trimethylsilyl)benzene-1,2-dithiol, $H_2$(tmsdt), in a water/methanol mixture in the presence of potassium *tert*-butoxide produced green crystals of [M(tren)(bdt)]$(PF_6)_{1/2}(Cl)_{1/2}\cdot H_2O$ (**1**$(PF_6)_{1/2}(Cl)_{1/2}\cdot H_2O$, M = Co; **2**$(PF_6)_{1/2}(Cl)_{1/2}\cdot H_2O$, M = Cr) and [M(tren)(tmsdt)]$(PF_6)_{1/2}(Cl)_{1/2}\cdot H_2O$ (**1a**$(PF_6)_{1/2}(Cl)_{1/2}\cdot H_2O$, M = Co; **2a**$(PF_6)_{1/2}(Cl)_{1/2}\cdot H_2O$, M = Cr), respectively, upon addition of $KPF_6$. The structures of **1**$(PF_6)_{1/2}(Cl)_{1/2}\cdot H_2O$ and **2**$(PF_6)_{1/2}(Cl)_{1/2}\cdot H_2O$ have been determined by X-ray crystallography. Octahedral **1** and **1a** are diamagnetic whereas **2** and **2a** possess an $S = {}^3/_2$ ground state. Cyclic voltammetry of **1a** and **2a** in $CH_2Cl_2$ solution established that both species undergo a reversible one-electron oxidation generating the stable dications $[Co^{III}(tren)(tmsdt^{\bullet})]^{2+}$ ($S = {}^1/_2$) and $[Cr^{III}(tren)(tmsdt^{\bullet})]^{2+}$ ($S = 1$) where $(tmsdt^{\bullet})^{1-}$ represents the $\pi$ radical monoanion of oxidized $(tmsdt)^{2-}$. The electrochemical oxidations are ligand centered processes. These dications have been investigated by UV−vis and EPR spectroscopy and density functional calculations using the B3LYP functional. The *S,S′*-coordinated benzene-1,2-dithiolate(1-) radical has been identified and unambiguously characterized. Comparison with the corresponding *o*-benzosemiquinonate(1-) complexes shows that the *S,S′*-coordinated benzene-1,2-dithiolate(1-) radical is a sulfur centered radical whereas its oxygen containing analogue carries ∼65% of the spin density on the six-membered ring.

## Introduction

In the past *O,O′*-coordinated *o*-benzosemiquinonato(1-) $\pi$ radical ligands $(sq^{\bullet})^{1-}$ have been most clearly identified and fully characterized in octahedral complexes of cobalt(III) and chromium(III)[1,2] where a single paramagnetic semiquinonate(1-) $\pi$ radical ($S_{rad} = {}^1/_2$) is *O,O′*-coordinated to a $M(tetramineN_4)^{3+}$ fragment (M = $Co^{III}$, $Cr^{III}$) yielding the octahedral dications $[Co^{III}(trien)(sq^{\bullet})]^{2+}$ and $[Cr^{III}(tren)(sq^{\bullet})]^{2+}$ (trien = triethylenetetramine, tren = tris(2-aminoethyl)amine). $[Co^{III}(trien)(3,5\text{-}DTBsq^{\bullet})]Cl_2$ ($S = {}^1/_2$) is one of the earliest examples (1976),[3] whereas $[Cr^{III}(tren)(3,6\text{-}DTBsq^{\bullet})](PF_6)_2$ is probably the most thoroughly studied, recent example (1998, 2004).[4,5] Structurally the $(sq^{\bullet})^{1-}$ oxidation level has been established because of relatively short C−O distances at ∼1.30 Å as compared with those reported for catecholates at ∼1.35 Å.[1,2] In addition, a typical quinoid-type distortion of the benzene ring is observed comprising two short C−C bonds at ∼1.36 Å and four long ones at ∼1.43 Å. The electronic structures of both *o*-semiquinonate complexes have been studied in great detail by variable temperature magnetochemistry, electron spin resonance (ESR), X-ray absorption (XAS),[6] and electronic absorption spectroscopy. In addition, McCusker et al. have corroborated the presence of a ligand $\pi$ radical and a chromium(III) ion in $[Cr^{III}(tren)(sq^{\bullet})](PF_6)_2$ by an elegant, in depth density functional theoretical study.[5] They established that a $Cr^{III}$ ($S = {}^3/_2$) ion is antiferromagnetically coupled to the semiquinonate ($S_{rad} = {}^1/_2$) giving rise to the observed triplet ground state. Population analyses showed α and $\beta$ spin densities at the Cr ion and the semiquinonate ligand, respectively.

In this report we employ the same combination of experimental methods (X-ray crystallography, UV−vis-, electron paramagnetic resonance (EPR)-spectroscopy, electrochemistry) and density functional theory (DFT) to establish unambiguously the presence of an *S,S′*-coordinated

*To whom correspondence should be addressed. E-mail: wieghardt@mpi-muelheim.mpg.de.

(1) Pierpont, C. G.; Buchanan, R. M. *Coord. Chem. Rev.* **1981**, *38*, 45.
(2) (a) Pierpont, C. G. *Coord. Chem. Rev.* **2001**, *216−217*, 99. (b) Pierpont, C. G. *Coord. Chem. Rev.* **2001**, *219−221*, 415. (c) Pierpont, C. G.; Lange, C. W. *Pure Appl. Chem.* **1994**, *41*, 331. (d) Pierpont, C. G.; Lange, C. W. *Prog. Inorg. Chem.* **1994**, *41*, 331. (e) Pierpont, C. G.; Larsen, S. K.; Boone, S. R. *Pure Appl. Chem.* **1988**, *60*, 1331.
(3) Wicklund, P. A.; Beckmann, L. S.; Brown, D. G. *Inorg. Chem.* **1976**, *15*, 1996.
(4) Wheeler, D. E.; McCusker, J. K. *Inorg. Chem.* **1998**, *37*, 2296.
(5) Rodriguez, J. H.; Wheeler, D. E.; McCusker, J. K. *J. Am. Chem. Soc.* **1998**, *120*, 12051.
(6) Milsmann, C.; Levina, A.; Harris, H. H.; Foran, G. J.; Turner, P.; Lay, P. A. *Inorg. Chem.* **2006**, *45*, 4743.


Published on Web 05/11/2009

benzene-1,2-dithiolate(1-) $\pi$ radical in the two species $[Co^{III}(tren)(tmsdt^{\bullet})]^{2+}$ and $[Cr^{III}(tren)(tmsdt^{\bullet})]^{2+}$ (Scheme 1). Surprisingly, octahedral mono(dithiolene) metal complexes containing a ligand $\pi$ radical monoanion have not been reported.[7] The calculated molecular and electronic structures of the uncoordinated molecules benzene-1,2-dithiol ($H_2L_{S,S}$) and its deprotonated one-electron oxidized radical form ($HL_{S,S}^{\bullet}$) are shown in Scheme 2.[8] The structural changes within the benzene ring on going from $H_2L_{S,S}$ to $HL_{S,S}^{\bullet}$ are small and will often be inside the estimated standard deviations ($3\sigma$) of the C−C bonds of an X-ray crystallographic structure determination. The C−S bond length changes are often outside the experimental error limits. The large spin density at the deprotonated and protonated sulfur atoms in $HL_{S,S}^{\bullet}$ at 65% allows only a limited delocalization of spin density on the phenyl ring. Therefore, identifications of $\pi$ radical anions by X-ray crystallography have been met with limited success. This is quite different for the oxygen analogues, namely, the catecholates and the corresponding *o*-semiquinonates.[1,2] Here the quinoid-type distortion of the six-membered is often significant as is the observed shortening of the C−O bond on going from the catechol to the *o*-semiquinone. Remarkably, the spin density of an *o*-semiquinonate resides ~70% on the six membered ring, and only 30% is located on the two oxygen atoms.

Historically, the bis(dithiolene)metal and tris(dithiolene) metal complexes have been extensively studied[7] and only very recently have spectroscopic methods like S K-edge X-ray absorption spectroscopy been developed to the extent that the presence of a benezene-1,2-dithiolate(1-) $\pi$ radical in a coordination compound can be established beyond doubt.[9]

## Experimental Section

**Preparation of Complexes.** The following compounds were prepared according to literature procedures: $[Cr^{III}(tren)Cl_2]Cl$,[10] $[Co^{III}(tren)Cl_2]Cl$,[11] 3,6 bis(trimethylsilyl)benzene 1,2 dithiol.[12]

**$[Co^{III}(tren)(bdt)](PF_6)_{1/2}(Cl)_{1/2}\cdot H_2O$ ($1(PF_6)_{1/2}(Cl)_{1/2}\cdot H_2O$).** A solution of $H_2$(bdt) (71 mg, 0.5 mmol) and potassium *tert*-butoxide (112 mg, 1 mmol) in methanol (10 mL) was added slowly with stirring to a solution of $[Co^{III}(tren)Cl_2]Cl$ (155 mg, 0.5 mmol) in water/methanol (1:1, 40 mL). The color of the solution changed from dark blue to olive green immediately. Potassium hexafluorophosphate (110 mg, 0.6 mmol) was added, and the solution was filtered. Upon reduction of the volume the dark olive green product was obtained as small needles. Yield: 115 mg (51%); ESI MS (pos. ions, MeCN): *m*/*z*: 345 $[Co(tren)(bdt)]^+$; Anal. Calcd for $C_{12}H_{24}Cl_{1/2}CoF_3N_4OP_{1/2}S_2$: C 31.77, H 5.33, N 12.35, Co 12.99; Found: C 31.42, H 5.36, N 12.18, Co 13.23. Crystals suitable for X-ray crystallography were

**Scheme 1.** Ligands and Complexes

| | | |
|---|---|---|
| $[Co^{III}(tren)(bdt)](PF_6)_{1/2}(Cl)_{1/2}\cdot H_2O$ | ($S = 0$) | **1**$(PF_6)_{1/2}(Cl)_{1/2}\cdot H_2O$ |
| $[Co^{III}(tren)(tmsdt)](PF_6)_{1/2}(Cl)_{1/2}\cdot H_2O$ | ($S = 0$) | **1a**$(PF_6)_{1/2}(Cl)_{1/2}\cdot H_2O$ |
| $[Cr^{III}(tren)(bdt)](PF_6)_{1/2}(Cl)_{1/2}\cdot H_2O$ | ($S = {}^3/_2$) | **2**$(PF_6)_{1/2}(Cl)_{1/2}\cdot H_2O$ |
| $[Cr^{III}(tren)(tmsdt)](PF_6)_{1/2}(Cl)_{1/2}\cdot MeOH$ | ($S = {}^3/_2$) | **2a**$(PF_6)_{1/2}(Cl)_{1/2}\cdot MeOH$ |

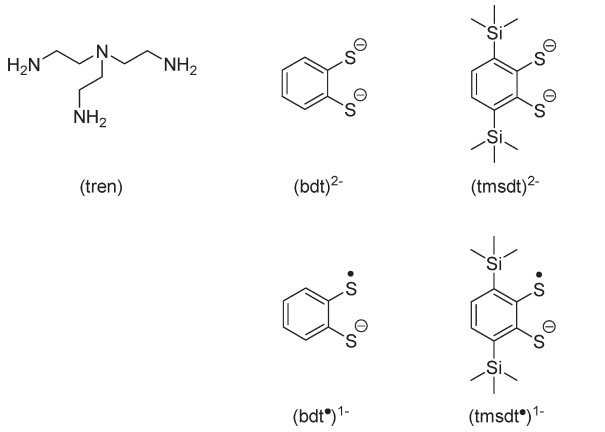


**Scheme 2.** Top: Calculated Molecular Structures of Uncoordinated Benzene-1,2-dithiol ($H_2L_{S,S}$) and Its Deprotonated One-Electron Oxidized Radical Form ($HL_{S,S}^{\bullet}$) in Comparison with Their Oxygen Analogues; Bottom: Mulliken Spin Densities of the Radicals $HL_{O,O}^{\bullet}$ and $HL_{S,S}^{\bullet}$

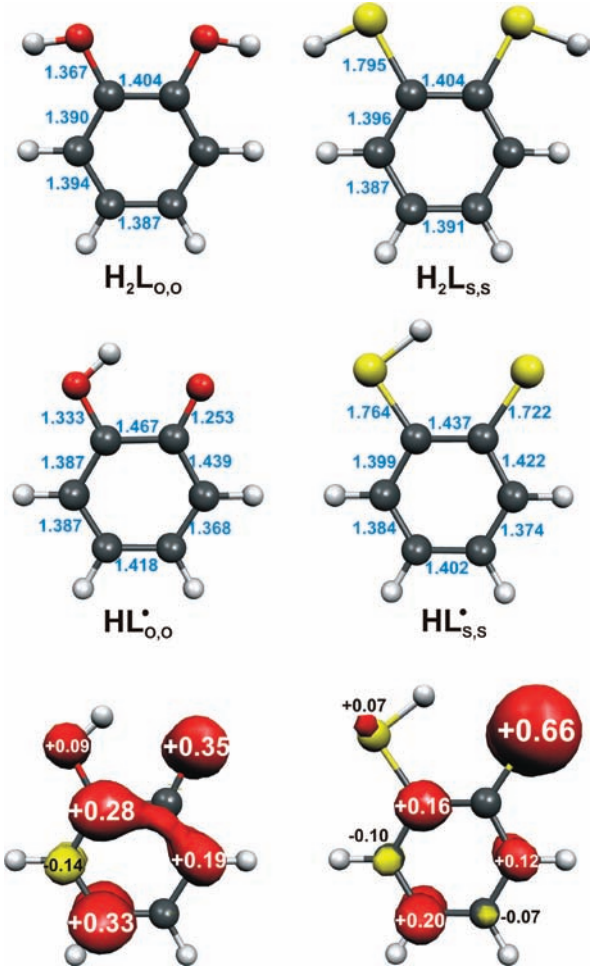


(7) Beswick, C. L.; Schulman, J. M.; Stiefel, E. I. *Prog. Inorg. Chem.* **2004**, *52*, 55.
(8) Ray, K.; Weyhermüller, T.; Neese, F.; Wieghardt, K. *Inorg. Chem.* **2005**, *44*, 5345–5360.
(9) (a) Szilagyi, R. K.; Lim, B. S.; Glaser, T.; Holm, R. H.; Hedman, B.; Hodgson, K. O.; Solomon, E. I. *J. Am. Chem. Soc.* **2003**, *125*, 9158. (b) Sarangi, R.; DeBeer George, S.; Jackson Rudd, D.; Szilagyi, R. K.; Ribas, X.; Rovira, C.; Almeida, M.; Hodgson, K. O.; Hedman, B.; Solomon, E. I. *J. Am. Chem. Soc.* **2007**, *129*, 2316. (c) Kapre, R. R.; Bothe, E.; Weyhermüller, T.; DeBeer George, S.; Wieghardt, K. *Inorg. Chem.* **2007**, *46*, 5642. (d) Ray, K.; DeBeer George, S.; Solomon, E. I.; Wieghardt, K.; Neese, F. *Chem.—Eur. J.* **2007**, *13*, 2783.
(10) Zipp, S. G.; Madan, S. K. *Inorg. Chem.* **1976**, *15*, 587.
(11) Kania, R.; Lewinski, K.; Sieklucka, B. *J. Chem. Soc., Dalton Trans.* **2003**, 1033–1040.
(12) Pap, J. S.; Benedito, F. L.; Bothe, E.; Bill, E.; DeBeer George, S.; Weyhermüller, T.; Wieghardt, K. *Inorg. Chem.* **2007**, *46*, 4187–4191.

**Table 1.** Crystallographic Data for $\mathbf{1}(PF_6)_{1/2}(Cl)_{1/2}\cdot H_2O$ and $\mathbf{2}(PF_6)_{1/2}(Cl)_{1/2}\cdot H_2O$

| | $\mathbf{1}(PF_6)_{1/2}(Cl)_{1/2}\cdot H_2O$ | $\mathbf{2}(PF_6)_{1/2}(Cl)_{1/2}\cdot H_2O$ |
|---|---|---|
| chem. formula | $C_{12}H_{24}Cl_{0.5}CoF_3N_4OP_{0.5}S_2$ | $C_{12}H_{24}Cl_{0.5}CrF_3N_4OP_{0.5}S_2$ |
| crystal size, $mm^3$ | $0.16 \times 0.04 \times 0.03$ | $0.18 \times 0.09 \times 0.04$ |
| fw | 453.61 | 446.68 |
| space group | $P2_1$, No. 4 | $P2_1$, No. 4 |
| $a$, Å | 7.0117(2) | 7.0883(2) |
| $b$, Å | 14.5876(5) | 14.6485(4) |
| $c$, Å | 17.3291(6) | 17.4787(5) |
| $\beta$, deg | 95.971(3) | 96.073(3) |
| $V$, Å | 1762.9(1) | 1804.68(9) |
| $Z$ | 4 | 4 |
| $T$, K | 100(2) | 100(2) |
| $\rho$ calcd, g $cm^{-3}$ | 1.709 | 1.644 |
| refl. collected/$2\Theta_{max}$ | 39364/66.36 | 52074/66.34 |
| unique refl./$I > 2\sigma(I)$ | 13373/10502 | 13684/10966 |
| no. of params/restr. | 449/6 | 445/6 |
| $\lambda$, Å /$\mu$ (K$\alpha$), $cm^{-1}$ | 0.71073/13.70 | 0.71073/10.21 |
| absolute structure param. | 0.019(8) | 0.017(10) |
| R1 [a]/goodness of fit [b] | 0.0459/ 1.018 | 0.0412/ 1.010 |
| wR2 [c] ($I > 2\sigma(I)$) | 0.0673 | 0.0643 |
| residual density, e $Å^{-3}$ | +0.78/−0.59 | +0.63/−0.44 |

[a] Observation criterion: $I > 2\sigma(I)$. $R1 = \sum||F_o| - |F_c||/\sum|F_o|$. [b] $GoF = \{\sum[w(F_o^2 - F_c^2)^2]/(n-p)\}^{1/2}$. [c] $wR2 = [\sum w(F_o^2 - F_c^2)^2/\sum w(F_o^2)^2]^{1/2}$ where $w = 1/\sigma^2(F_o^2) + (aP)^2 + bP$, $P = (F_o^2 + 2F_c^2)/3$.

grown by slow evaporation of solutions of the complex in methanol/water (3:1).

**$[Co^{III}(tren)(tmsdt)](PF_6)_{1/2}(Cl)_{1/2}\cdot H_2O$ ($\mathbf{1a}(PF_6)_{1/2}(Cl)_{1/2}\cdot H_2O$).** Because of the high air sensitivity of the ligand $H_2$(tmsdt) all steps were carried out under an argon blanketing atmosphere using degassed solvents. A solution of $H_2$(tmsdt) (103 mg, 0.36 mmol) and potassium *tert*-butoxide (90 mg, 0.8 mmol) in methanol (10 mL) was added slowly with stirring to a solution of $[Co^{III}(tren)Cl_2]Cl$ (111 mg, 0.36 mmol) in water/methanol (1:1, 30 mL). The color of the solution changed from dark blue to olive green immediately. Potassium hexafluorophosphate (75 mg, 0.4 mmol) was added, and the solvents were removed in vacuo. The green crude product was dissolved in diethylether and filtered in air. Upon evaporation of the solvent the product was obtained as an air-stable green powder. Yield: 103 mg (45%). Anal. Calcd for $C_{18}H_{40}Cl_{1/2}CoF_3N_4OP_{1/2}S_2Si_2$: C 36.16, H 6.74, N 9.37; found: C 35.67, H 6.61, N 8.94.

**$[Cr^{III}(tren)(bdt)](PF_6)_{1/2}(Cl)_{1/2}\cdot H_2O$ ($\mathbf{2}(PF_6)_{1/2}(Cl)_{1/2}\cdot H_2O$).** A solution of $H_2$(bdt) (71 mg, 0.5 mmol) and potassium *tert*-butoxide (112 mg, 1 mmol) in methanol (10 mL) was added slowly with stirring to a solution of $[Cr^{III}(tren)Cl_2]Cl$ (150 mg, 0.5 mmol) in water/methanol (4:3, 35 mL). The mixture was heated to reflux for 3 h, which caused a color change of the solution from pink to olive green. Potassium hexafluorophosphate (110 mg, 0.6 mmol) was added, and the solution was filtered. Upon reduction of the volume dark olive green crystals of product were obtained. Yield: 183 mg (84%); Anal. Calcd for $C_{12}H_{24}Cl_{1/2}CrF_3N_4OP_{1/2}S_2$: C 32.27, H 5.42, N 12.54, Cr 11.64; found: C 32.35, H 5.48, N 12.36, Cr 11.94.

**$[Cr^{III}(tren)(tmsdt)](PF_6)_{1/2}(Cl)_{1/2}\cdot MeOH$ ($\mathbf{2a}(PF_6)_{1/2}(Cl)_{1/2}\cdot MeOH$).** Because of the high air sensitivity of the ligand $H_2$(tmsdt) all steps were carried out under an argon blanketing atmosphere using degassed solvents. A solution of $H_2$(tmsdt) (143 mg, 0.5 mmol) and potassium *tert*-butoxide (135 mg, 1.2 mmol) in methanol (15 mL) was added slowly with stirring to a solution of $[Cr^{III}(tren)Cl_2]Cl$ (150 mg, 0.5 mmol) in water/methanol (1:1, 30 mL). The mixture was heated to reflux for 3 h, which caused a color change of the solution from pink to olive green. Potassium hexafluorophosphate (110 mg, 0.6 mmol) was added, and the solvents were removed in vacuum. The green crude product was dissolved in diethyl ether and filtered in air. Upon evaporation of the solvent the product was obtained as an air-stable green powder. Yield: 157 mg (64%). Anal. Calcd for $C_{19}H_{43}Cl_{1/2}CrF_3N_4OP_{1/2}S_2Si_2$: C 37.72, H 7.00, N 9.26; found: C 38.30, H 7.15, N 9.55.

**X-ray Crystallographic Data Collection and Refinement of the Structures.** A green single crystal of $\mathbf{1}(PF_6)_{1/2}(Cl)_{1/2}\cdot H_2O$ and a green brownish crystal of $\mathbf{2}(PF_6)_{1/2}(Cl)_{1/2}\cdot H_2O$ were coated with perfluoropolyether, picked up with nylon loops and mounted in the nitrogen cold stream of a Bruker-Nonius Kappa CCD diffractometer equipped with a Mo-target rotating-anode X-ray source. Graphite monochromated Mo K$\alpha$ radiation ($\lambda$ = 0.71073 Å) was used. Final cell constants were obtained from least-squares fits of several thousand strong reflections. Intensities of redundant reflections were used to correct for absorption using the program SADABS.[13] The structures were readily solved by Patterson methods and subsequent difference Fourier techniques. The Siemens ShelXTL[14] software package was used for solution and artwork of the structures, ShelXL97[15] was used for the refinement. All non-hydrogen atoms were anisotropically refined, and hydrogen atoms bound to carbon and nitrogen atoms were placed at calculated positions and refined as riding atoms with isotropic displacement parameters. Hydrogen atoms of the water molecules in $\mathbf{1}(PF_6)_{1/2}(Cl)_{1/2}\cdot H_2O$ and $\mathbf{2}(PF_6)_{1/2}(Cl)_{1/2}\cdot H_2O$ were localized from the difference map and were refined with constrained bond lengths using the DFIX instruction of ShelXL97. Crystallographic data of the compounds are listed in Table 1.

**Physical Measurements.** Cyclic voltammograms and square wave voltammograms in the range of −25 to 25 °C were recorded by using an EG&G Potentiostat/Galvanostat 273A. A three electrode cell was employed with a glassy-carbon working electrode, a glassy-carbon auxiliary electrode, and a Ag/$AgNO_3$ reference electrode (0.01 M $AgNO_3$ in $CH_3CN$). Ferrocene was added as an internal standard after completion of the measurements, and potentials are referenced versus the $Fc^+$/Fc couple. Controlled potential coulometric measurements were performed in a setup, which allows recording of absorption spectra in situ during electrolysis, by employing the same potentiostat, but using a Pt-grid as a working electrode. A Pt-brush was used as counter electrode and separated from the

(13) *SADABS*, 2006/1; Bruker AXS Inc.: Madison, WI, U.S.A., 2007.
(14) *ShelXTL*, 6.14; Bruker AXS Inc.: Madison, WI, U.S.A., 2003.
(15) G. M. Sheldrick *ShelXL97*; University of Göttingen: Göttingen, Germany, 1997.

working electrode compartment by a Vycor frit. An $Ag/AgNO_3$ (0.01 M $AgNO_3$ in $CH_3CN$) reference electrode was employed again. UV−vis spectra were measured on a Hewlett-Packard 8452A diode array spectrophotometer. Temperature-dependent magnetic susceptibilities were measured by using a SQUID magnetometer (MPMS Quantum Design) at 1.0 T (4−300 K). Underlying diamagnetism was corrected by using tabulated Pascal's constants. X-band EPR derivative spectra were recorded on a Bruker ELEXSYS E500 spectrometer equipped with the Bruker standard cavity (ER4102ST) and a helium flow cryostat (Oxford Instruments ESR 910). Microwave frequencies were calibrated with a Hewlett-Packard frequency counter (HP5352B), and the field control was calibrated with a Bruker NMR field probe (ER035M). The spectra were simulated with the program GFIT (by Eckhard Bill) for the calculation of powder spectra with effective $g$ values and anisotropic line widths (Gaussian line shapes were used).

**Calculations.** All DFT calculations were performed with the ORCA[16] program package. The geometry optimizations of the complexes and single-point calculations on the optimized geometries were carried out using the B3LYP[17] functional. This hybrid functional often gives better results for transition metal compounds than pure gradient-corrected functionals, especially with regard to metal−ligand covalency.[18] The all-electron Gaussian basis sets were those developed by the Ahlrichs group.[19,20] Triple-$\zeta$ quality basis sets TZV(P) with one set of polarization functions on the metals and on the atoms directly coordinated to the metal center were used.[20] For the carbon and hydrogen atoms, slightly smaller polarized split-valence SV(P) basis sets were used, that were of double-$\zeta$ quality in the valence region and contained a polarizing set of d-functions on the non-hydrogen atoms.[19] Auxiliary basis sets used to expand the electron density in the resolution-of-the-identity (RI) approach were chosen,[21] where applicable, to match the orbital basis. The SCF calculations were tightly converged ($1 \times 10^{-8}$ $E_h$ in energy, $1 \times 10^{-7}$ $E_h$ in the density change, and $1 \times 10^{-7}$ in maximum element of the DIIS error vector). The geometry optimizations for all complexes were carried out in redundant internal coordinates without imposing symmetry constraints. In all cases the geometries were considered converged after the energy change was less than $5 \times 10^{-6}$ $E_h$, the gradient norm and maximum gradient element were smaller than $1 \times 10^{-4}$ $E_h$ $Bohr^{-1}$ and $3 \times 10^{-4}$ $E_h$ $Bohr^{-1}$, respectively, and the root-mean square and maximum displacements of all atoms were smaller than $2 \times 10^{-3}$ Bohr and $4 \times 10^{-3}$ Bohr, respectively. Throughout this paper we describe our computational results by using the broken-symmetry (BS) approach by Ginsberg[22] and Noodleman.[23] Because several broken symmetry solutions to the spin-unrestricted Kohn−Sham equations may be obtained, the general notation BS($m$,$n$)[24] has been adopted, where $m$ ($n$) denotes the number of spin-up (spin-down) electrons at the two interacting fragments. Canonical and corresponding orbitals,[25] as well as spin density plots were generated with the program Molekel.[26]

## Results and Discussion

**Synthesis and Characterization of Complexes.** Slow addition of 1 equiv of benzene-1,2-dithiol, $H_2$(bdt), or 3,6-bis(trimethylsilyl)benzene-1,2-dithiol, $H_2$(tmsdt), dissolved in methanol to a solution of $[Co^{III}(tren)Cl_2]Cl$ in the presence of 2 equiv of potassium *tert*-butoxide, $KO^tBu$, produced an olive green solution from which upon addition of excess $KPF_6$ and slow evaporation of the solvent dark green crystals of $[Co^{III}(tren)(bdt)](PF_6)_{1/2}(Cl)_{1/2}\cdot H_2O$, **1**$(PF_6)_{1/2}(Cl)_{1/2}\cdot H_2O$, and $[Co^{III}(tren)(tmsdt)](PF_6)_{1/2}(Cl)_{1/2}\cdot H_2O$, **1a**$(PF_6)_{1/2}(Cl)_{1/2}\cdot H_2O$, were obtained in moderate yields, respectively. The syntheses were carried out under an argon blanketing atmosphere. Magnetic susceptibility measurements established that both compounds are diamagnetic ($S$ = 0 ground state).

The corresponding complexes $[Cr^{III}(tren)(bdt)](PF_6)_{1/2}(Cl)_{1/2}\cdot H_2O$, **2**$(PF_6)_{1/2}(Cl)_{1/2}\cdot H_2O$, and $[Cr^{III}(tren)(tmsdt)](PF_6)_{1/2}(Cl)_{1/2}\cdot MeOH$, **2a**$(PF_6)_{1/2}(Cl)_{1/2}\cdot MeOH$, were prepared as described above for the cobalt complexes by using $[Cr^{III}(tren)Cl_2]Cl$ as starting material. Both complexes are paramagnetic and possess an $S = {}^3/_2$ ground state. The effective magnetic moments, $\mu_{eff}$, of **2** and **2a** are virtually temperature independent from 50 to 290 K at 3.80 and 4.08 $\mu_B$, respectively.

Figure 1 displays the X-band EPR spectrum of **2a** in a frozen $CH_2Cl_2$/toluene (1:1) mixture at 10 K, which confirms the expected quartet ground state. The observed effective $g$-values are typical for an electronic spin of $S = {}^3/_2$ with moderately large zero field splitting (ZFS) and large rhombicity ($kT \approx 7$ $cm^{-1}$ at 10 K $> D > h\nu \approx$ 0.3 $cm^{-1}$ at X-band; $E/D \gg 0$). They originate from two Kramers doublets, $|3/2, \pm 1/2\rangle$ and $|3/2, \pm 3/2\rangle$, which are both thermally populated, if the ZFS is small versus $kT$. For the limiting case of axial symmetry ($E/D = 0$) transitions within the $m_s = \pm 3/2$ doublet are forbidden and, therefore, EPR silent. In this situation, only two effective $g'$-values at $g'_{\parallel,1/2} = 4.0$ and $g'_{\perp,1/2} = 2.0$ are expected in the resulting spectrum. For higher rhombicity the $g'_{\parallel,1/2} = 4.0$ signal is split into two separate $g'$-values. This is clearly the case here. The $g'$-values are observed at $g'_{y,1/2} = 5.09$ and $g'_{x,1/2} = 2.57$ in the spectrum, whereas the third $g$-value of this $m_s = \pm 1/2$ doublet shifts only slightly to $g'_{z,1/2} = 1.64$. Additionally, the transitions within the $m_s = \pm 3/2$ doublet become allowed at high $E/D$ and signals are observed at $g'_{z,3/2} = 5.66$ and $g'_{x,3/2} = 1.48$. The third $g'$-value of this doublet is expected to be below $g' = 1.2$ and, hence, was not detected within the experimentally available field range. The relative intensities of the signals for $g'_{y,1/2}$ and the $g'_{z,3/2}$ are a very sensitive probe for the size of the ZFS parameter $D$, since the thermal population of the two Kramers doublets is determined by the energy splitting of $2D$ (see inset Figure 1).

(16) Neese, F., *Orca*. Orca − an ab initio, DFT and Semiempirical Electronic Structure Package, Version 2.6, Revision 4; Institut für Physikalische und Theoretische Chemie, Universität Bonn, Bonn, Germany, May 2007.
(17) (a) Becke, A. D. *J. Chem. Phys.* **1986**, *84*(8), 4524. (b) Becke, A. D. *J. Chem. Phys.* **1993**, *98*(7), 5648. (c) Lee, C. T.; Yang, W. T.; Parr, R. G. *Phys. Rev. B* **1988**, *37*, 785.
(18) Neese, F.; Solomon, E. I. In *Magnetoscience: From Molecules to Materials*; Miller, J. S., Drillon, M., Eds.; Wiley: New York, 2002; Vol. *4*, p 345.
(19) Schäfer, A.; Horn, H.; Ahlrichs, R. *J. Chem. Phys.* **1992**, *97*(4), 2571.
(20) Schäfer, A.; Huber, C.; Ahlrichs, R. *J. Chem. Phys.* **1994**, *100*(8), 5829.
(21) (a) Eichkorn, K.; Weigend, F.; Treutler, O.; Ahlrichs, R. *Theor. Chem. Acc.* **1997**, *97*, 119. (b) Eichkorn, K.; Treutler, O.; Öhm, H.; Häser, M.; Ahlrichs, R. *Chem. Phys. Lett.* **1995**, *240*, 283. (c) Eichkorn, K.; Treutler, O.; Öhm, H.; Häser, M.; Ahlrichs, R. *Chem. Phys. Lett.* **1995**, *242*, 652.
(22) Ginsberg, A. P. *J. Am. Chem. Soc.* **1980**, *102*, 111.
(23) Noodleman, L.; Peng, C. Y.; Case, D. A.; Mouesca, J. M. *Coord. Chem. Rev.* **1995**, *144*, 199.
(24) Kirchner, B.; Wennmohs, F.; Ye, S.; Neese, F. *Curr. Opin. Chem. Biol.* **2007**, *11*, 134.
(25) Neese, F. *J. Phys. Chem. Solids* **2004**, *65*, 781.
(26) *Molekel*; Advanced Interactive 3D-Graphics for Molecular Sciences, available under http:\\www.cscs.ch/molekel/.

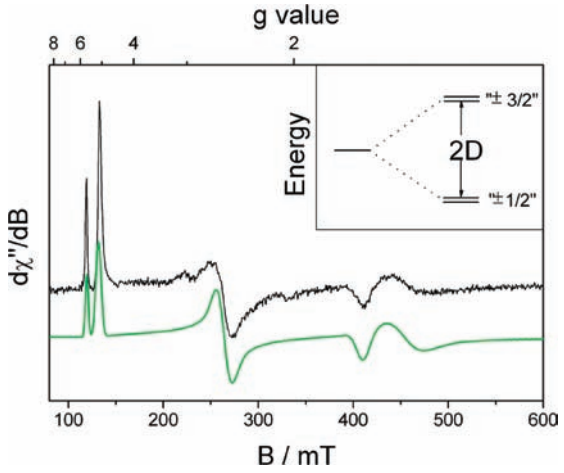


**Figure 1.** X-band EPR spectrum of **2a** (black) in frozen $CH_2Cl_2$/toluene (0.2 mM, 10.2 K, frequency = 9.44 GHz, modulation = 1 mT, power = 0.1 mW); simulated spectrum (green). The inset shows the zero-field splitting of the two Kramers doublets.

With these assumptions the spectrum was successfully simulated with intrinsic $g$-values of $g = 2.00, 2.00$, and 1.98, a zero-field splitting parameter $D$ of 0.8 $cm^{-1}$, and a rhombicity $E/D$ of 0.23. A distribution of the rhombicity ($E/D$-strain) with a width of $\sigma(E/D) = 0.1$ was imposed to model the line width. This line broadening is due to microheterogeneity in the sample. These zero-field parameters are in accord with the values found for other $Cr^{III}$ coordination compounds with the general electronic configuration $(d_{xz})^1(d_{yz})^1(d_{x^2-y^2})^1$ and $S = {}^3/_2$.[27]

**Crystal Structure Determinations.** The structures of complexes $\mathbf{1}(PF_6)_{1/2}(Cl)_{1/2}\cdot H_2O$ and $\mathbf{2}(PF_6)_{1/2}(Cl)_{1/2}\cdot H_2O$ have been determined by X-ray crystallography at 100(2) K. Crystallographic details are provided in Table 1. Both compounds are isostructural; they crystallize in the chiral, monoclinic space group $P2_1$. Two crystallographically independent cations are present in the unit cell, which exhibit very similar structural parameters, apart from significantly differing folding angles of the dithiolene ligand (see below). The ligands adopt an octahedral geometry around the central metal ion, with the dithiolene ligand occupying two equatorial coordination sites in *cis*-configuration.

The structures of the two crystallographically independent cations of **1** are shown in Figure 2a; Table 2 summarizes important bond distances and angles. The average C−S bond length in **1** is relatively long at 1.763(3) Å indicating the presence of a closed-shell benzene-1,2-dithiolate(2-) ligand.[8] As expected, this is also corroborated by the equidistant aromatic C−C bond lengths in the benzene ring. Thus, the central Co ion possesses a +III formal oxidation state ($d^6$, $S = 0$). All Co−N bond lengths of the neutral tren ligand are $<2$ Å implying a diamagnetic, low-spin $Co^{III}$ center with a $d^6$ electronic configuration, in agreement with the magnetic measurements. The equatorial Co−N bonds (1.991(2) Å) are elongated compared to the axial ones (1.970(2) Å) because of the strong structural trans-effect of the sulfur donor atoms of the dithiolate(2-) ligand.

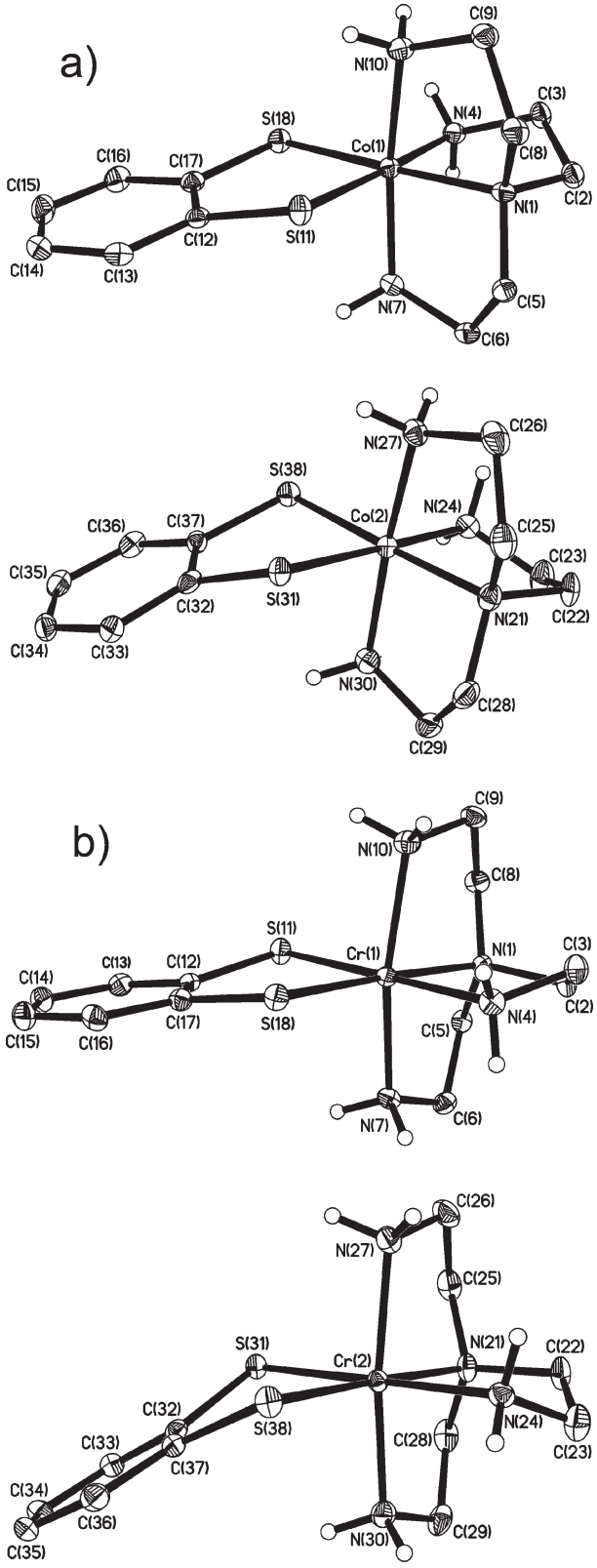


**Figure 2.** Structures and labeling schemes for the two crystallographically independent monocations (a) **1** and (b) **2**. Thermal ellipsoids are drawn at the 50% probability level. C−H hydrogen atoms are omitted for clarity.

Figure 2b shows the structures of the two crystallographically independent cations of **2**; Table 2 summarizes

(27) (a) Singer, L. S. J. *Chem. Phys.* **1955**, *23*, 379. (b) Mabbs, F. E.; Collison, D. *Electron Paramagnetic Resonance of d Transition Metal Compounds*; Elsevier: Amsterdam, 1992.(c) Shaham, N.; Cohen, H.; Meyerstein, D.; Bill, E. *J. Chem. Soc., Dalton Trans.* **2000**, 3082. (d) Pedersen, E.; Toftlund, H. *Inorg. Chem.* **1974**, *13*, 1603. (e) Goodson, P. A.; Glerup, J.; Hodgson, D. J.; Jensen, N. B.; Michelsen, K. *J. Chem. Soc., Dalton Trans.* **2001**, 2783.

**Table 2.** Selected Bond Distances (Å) and Angles (deg) in **1** and **2**

| | | | | |
|---|---|---|---|---|
| Complex **1** | Co(1′)−N(1′) | 1.994(2) | Co(1)−N(1) | 1.968(2) |
| | Co(1′)−N(2′) | 1.976(2) | Co(1)−N(2) | 1.989(2) |
| | Co(1′)−N(3′) | 1.996(2) | Co(1)−N(3) | 1.992(2) |
| | Co(1′)−N(4′) | 1.963(2) | Co(1)−N(4) | 1.972(2) |
| | Co(1′)−S(1′) | 2.2585(7) | Co(1)−S(1) | 2.2636(7) |
| | Co(1′)−S(2′) | 2.2317(7) | Co(1)−S(2) | 2.2414(7) |
| | S(1′)−C(1′) | 1.755(2) | S(1)−C(1) | 1.760(3) |
| | S(2′)−C(6′) | 1.765(2) | S(2)−C(6) | 1.766(2) |
| | C(1′)−C(2′) | 1.402(3) | C(1)−C(2) | 1.399(3) |
| | C(2′)−C(3′) | 1.392(4) | C(2)−C(3) | 1.389(4) |
| | C(3′)−C(4′) | 1.385(4) | C(3)−C(4) | 1.384(4) |
| | C(4′)−C(5′) | 1.387(4) | C(4)−C(5) | 1.393(4) |
| | C(5′)−C(6′) | 1.401(4) | C(5)−C(6) | 1.400(4) |
| | C(6′)−C(1′) | 1.403(3) | C(6)−C(1) | 1.409(3) |
| | $\varphi'$ | 10.33 | $\varphi$ | 29.19 |
| Complex **2** | Cr(1′)−N(1′) | 2.1214(18) | Cr(1)−N(1) | 2.0895(19) |
| | Cr(1′)−N(2′) | 2.0919(17) | Cr(1)−N(2) | 2.0956(18) |
| | Cr(1′)−N(3′) | 2.1006(17) | Cr(1)−N(3) | 2.0978(17) |
| | Cr(1′)−N(4′) | 2.0881(17) | Cr(1)−N(4) | 2.0991(18) |
| | Cr(1′)−S(1′) | 2.3601(6) | Cr(1)−S(1) | 2.3636(6) |
| | Cr(1′)−S(2′) | 2.3369(6) | Cr(1)−S(2) | 2.3494(6) |
| | S(1′)−C(1′) | 1.761(2) | S(1)−C(1) | 1.768(2) |
| | S(2′)−C(6′) | 1.773(2) | S(2)−C(6) | 1.773(2) |
| | C(1′)−C(2′) | 1.409(3) | C(1)−C(2) | 1.400(3) |
| | C(2′)−C(3′) | 1.381(3) | C(2)−C(3) | 1.388(3) |
| | C(3′)−C(4′) | 1.392(3) | C(3)−C(4) | 1.382(3) |
| | C(4′)−C(5′) | 1.386(3) | C(4)−C(5) | 1.386(3) |
| | C(5′)−C(6′) | 1.400(3) | C(5)−C(6) | 1.402(3) |
| | C(6′)−C(1′) | 1.404(3) | C(6)−C(1) | 1.406(3) |
| | $\varphi'$ | 10.45 | $\varphi$ | 30.34 |

important bond distances and angles. The average C−S bond length in **2** is again long at 1.769(3) Å indicating the presence of a closed-shell benzene-1,2-dithiolate(2-) ligand. The C−C bond lengths of the benzene rings are also equidistant within experimental error. The Cr−N distances range from 2.088(2) Å to 2.121(2) Å, which is typical for the tren ligand coordinated to a $Cr^{III}$ central metal ion.[4,5,28]

An interesting feature in both structures is the folding angle $\varphi$ between the mean S−C−C−S trapezoidal plane and the S−M−S plane, which results in a folding of the dithiolene ligand about the S−S vector (Figure 3). It is apparent from the structures of both cations that steric reasons for the ligand folding can be ruled out. Instead, the angle $\varphi$ may provide insight into the $\pi$ interaction between the dithiolene ligand and the central metal ion and, therefore, may help to elucidate the electronic structure. For complexes with strong $\pi$ interactions between the sulfur donor atoms and the central metal, ion a planar arrangement with an angle $\varphi$ of 180° is expected, maximizing the overlap between the metal $t_{2g}$ orbitals, which possess $\pi$ symmetry in octahedral systems, and the $\pi$ system of the ligand. In the absence of $\pi$ interactions the five-membered ring formed by the metal and the dithiolene can adopt a folded geometry. The observed flexibility in $\varphi$ for both monocations **1** and **2** in the solid state indicates the *absence* of strong $\pi$ interactions between the dithiolate(2-) ligand and metal ion. For **1** this is not surprising because it contains a low-spin $Co^{III}$ ion and a dianionic dithiolene ligand. The ligand can, in this situation, only act as a $\pi$ donor, but since the $t_{2g}$ orbitals of the $Co^{III}$ center are completely filled,

(28) (a) Guo, D.; McCusker, J. K. *Inorg. Chem.* **2007**, *46*, 3257. (b) Möller, K.; Näther, C.; Bannwarth, A.; Bensch, W. *Z. Anorg. Allg. Chem.* **2007**, *633*, 2635.

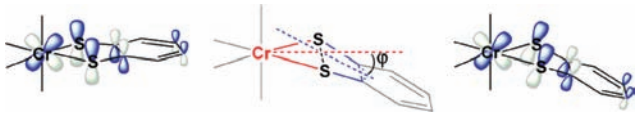


**Figure 3.** Representation of the dihedral angle $\varphi$ between the mean S−C−C−S trapezoidal plane (blue) and the S−Cr−S plane (red), which results in a bending of dithiolate ligand about the S−S vector (middle) and its influence on the $\pi$ interaction between the metal $d_{xz}$ and the ligand $\pi^*$ orbital (left $\varphi$ = 0°, right $\varphi$ = 25°).

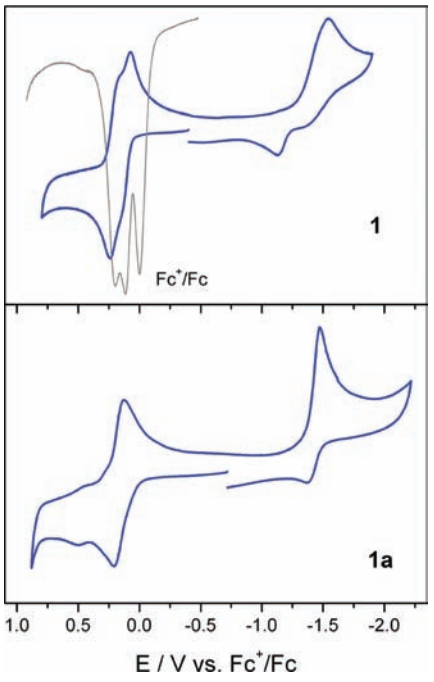


**Figure 4.** Cyclic voltammogram of **1** in MeCN (top) and **1a** in $CH_2Cl_2$ (bottom); 22 °C, 0.10 M $[N(n\text{-}Bu)_4]PF_6$, scan rate 200 mV $s^{-1}$, glassy carbon working electrode. The gray line in the upper spectrum represents the square wave voltammogram of **1**, resolving the two redox waves. The peak at 0 V is due to the internal standard ferrocene.

significant $\pi$ bonding is not possible. For **2** the situation is different. In this case, the $t_{2g}$ set is only half-filled, but the fact that there appears to be the same flexibility in $\varphi$ indicates again the absence of significant $\pi$ bonding. A straightforward explanation is that the half filled $t_{2g}$ set on the $Cr^{III}$ ion is much higher in energy than the filled $\pi$ orbitals of the ligand, thus preventing significant covalent interactions. This is shown to be the case below by the density functional theoretical calculations.

**Spectroelectrochemistry.** Cyclic voltammograms (CV) of **1** and **1a** have been recorded in acetonitrile and $CH_2Cl_2$ solution, respectively, containing 0.10 M $[N(n\text{Bu})_4]PF_6$ as the supporting electrolyte by using a glassy carbon working electrode. Ferrocene was used as internal standard, and all potentials are referenced against the ferrocenium/ferrocene couple ($Fc^+$/Fc). Figure 4 shows the cyclic voltammograms of **1** and **1a**. Both complexes show an irreversible reduction-wave at approximately 1.5 V, which was not investigated in further detail. This process is expected to involve a metal-centered reduction ($Co^{III} \rightarrow Co^{II}$). In addition, the CV of compound **1** shows two very close redox-couples at ~0.15 V, which are not resolved, but their square wave voltammograms show two reversible electron transfer processes at 0.20 and 0.12 V. Controlled-potential coulometry established

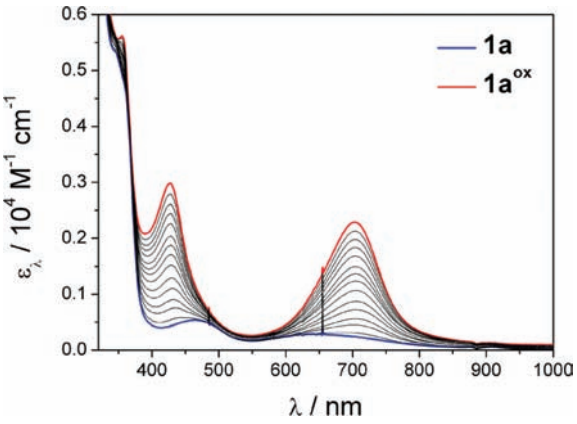


**Figure 5.** Spectral changes in the electronic absorption spectrum upon electrochemical oxidation of **1a** (blue) to $\mathbf{1a^{ox}}$ (red) at +400 mV in $CH_2Cl_2$; 0.10 M $[N(n\text{-}Bu)_4]PF_6$, −25 °C.

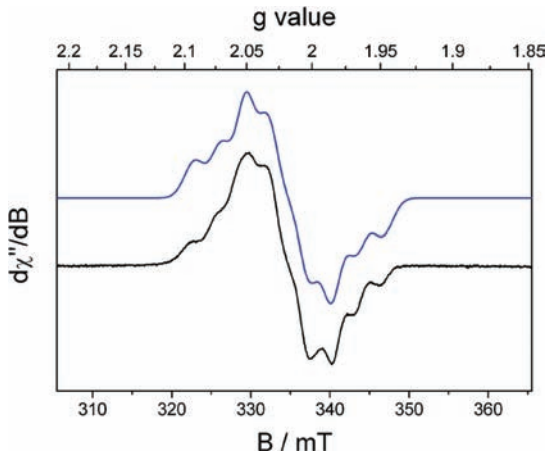


**Figure 6.** X-band EPR spectrum (black) of electrochemically generated $\mathbf{1a^{ox}}$ in frozen $CH_2Cl_2$; 0.2 mM, 10.0 K, frequency = 9.45 GHz, modulation = 10 G, power = 0.02 mW. The simulation is shown in blue.

that the sum of these two processes corresponds to a one-electron oxidation of the compound. Unfortunately, the product of the oxidation was found to be unstable on the time scale of the coulometric experiment. The higher solubility of $\mathbf{1a}(PF_6)$ allowed us to perform electrochemical experiments in $CH_2Cl_2$ which in contrast to MeCN is a less coordinating solvent. The trimethylsilyl substituents are ideally suited to stabilize the oxidized form of the compound by adding steric protection to the system. In fact, **1a** shows only a single, reversible redox wave at 0.17 V, that corresponds to a one-electron oxidation, as shown by controlled-potential coulometry at −25 °C. The dicationic product $\mathbf{1a^{ox}}$ is stable under these conditions and was investigated using spectroelectrochemistry.

The spectral changes in the absorption spectra of **1a** during the electrochemical one-electron oxidation in $CH_2Cl_2$ (0.10 M $[N(n\text{-}Bu)_4]PF_6$) solution at −25 °C are shown in Figure 5. The starting material **1a** exhibits only two relatively weak transitions in the region between 400−1000 nm at 463 nm ($\varepsilon$ = 540 $M^{-1}$ $cm^{-1}$) and 646 nm (280 $M^{-1}$ $cm^{-1}$), which, from their low extinction coefficients $\varepsilon_\lambda$, can be interpreted as d-d transitions. This is expected for an octahedral, low-spin $d^6$-system ($Co^{III}$) with a closed shell, dianionic dithiolene ligand. Upon oxidation two new bands appear at 427 nm (2990 $M^{-1}$ $cm^{-1}$) and 702 nm (2290 $M^{-1}$ $cm^{-1}$), which show a much higher $\varepsilon_\lambda$ and, therefore, are either ligand-to-metal (LMCT) or metal-to-ligand charge-transfer bands (MLCT).

The X-band EPR spectrum of the electrochemically generated dication $\mathbf{1a^{ox}}$ in $CH_2Cl_2$ at 10 K is shown in Figure 6; it indicates an $S = 1/2$ ground state. This spectrum has been successfully simulated using the following parameters: $g_x = 2.036$, $g_y = 2.018$, $g_z = 2.000$ ($g_{iso} = 2.018$) and $^{59}Co$ hyperfine coupling constants $A_{xx} = 5$ G, $A_{yy} = 32$ G, $A_{zz} = 5$ G ($A_{iso} = 14$ G). The low anisotropy of the rhombic signal is quite typical for dithiolene radicals.[29] The relatively high g-anisotropy for an organic radical is due to the fact that the unpaired electron in dithiolene radicals is predominantly located on the sulfur atoms.[8,30] This indicates that the unpaired electron in $\mathbf{1a^{ox}}$ resides mainly in a ligand orbital. This is further corroborated by the relatively weak hyperfine coupling to $^{59}Co$ ($I = {}^7/_2$). The isotropic coupling constant of 14 G is very similar to the one previously reported for an *S*-coordinated phenylthyil radical (10 G).[31] It is also similar to the corresponding isotropic $^{59}Co$ coupling constant in $[Co^{III}(trien)(3,5\text{-di-}tert\text{-butylbenzosemiquinonato})]^{2+}$ at 9.76 G reported in ref 3. Also, it is reasonable that this coupling is larger in $\mathbf{1a^{ox}}$ than in its oxygen analogue[3] because the Co−S bonds are more covalent than the Co−O bonds. The increase of coupling in going from phenylthyil to dithiolene radical parallels the trend observed in phenoxyl versus semiquinonato radicals.[32] Therefore, complex $\mathbf{1a^{ox}}$ is best formulated as $[Co^{III}(tren)(tmsdt^{\bullet})]^{2+}$, which implies a $d^6$ low-spin configuration at the cobalt ion, and consequently, the oxidation from **1a** to $\mathbf{1a^{ox}}$ must be ligand centered.

For the chromium complex **2** no reversible electrochemical processes were observed by cyclic voltammetry in the range from −1.8 V to +1.5 V relative to the internal ferrocene standard (MeCN, 0.10 M $[N(n\text{-}Bu)_4]PF_6$ glassy carbon working electrode). Similar to the cobalt complexes, the derivative carrying a $(tmsdt)^{2-}$ ligand, namely, **2a**, shows a much higher stability upon oxidation. A reversible one-electron transfer redox wave at 0.08 V in $CH_2Cl_2$ as shown in Figure 7 is observed.

Controlled potential coulometry conducted at −25 °C generated the dicationic oxidized species $\mathbf{2a^{ox}}$. The spectrum of $\mathbf{2a^{ox}}$ is shown in Figure 8. The spectrum of the starting material **2a** shows two peaks at 330 nm (5450 $M^{-1}$ $cm^{-1}$) and 388 nm (1800 $M^{-1}$ $cm^{-1}$), which are most likely LMCT transitions to the $t_{2g}$ set. The relatively high energy of these transitions indicate, that the ligand $\pi^*$-orbitals and the metal d orbitals are very different in energy. Upon oxidation of the compound three new peaks appear in the visible region (436, 505, and 699 nm). These changes are very similar to the ones observed in the catecholate-semiquinone oxidation[33] of the

(29) (a) Ray, K.; Weyhermüller, T.; Goossens, A.; Craje, M. W. J.; Wieghardt, K. *Inorg. Chem.* **2003**, *42*, 4082. (b) Ray, K.; Bill, E.; Weyhermüller, T.; Wieghardt, K. *J. Am. Chem. Soc.* **2005**, *127*, 5641.
(30) van Gastel, M.; Lubitz, W.; Lassmann, G.; Neese, F. *J. Am. Chem. Soc.* **2004**, *126*, 2237.
(31) Kimura, S.; Bill, E.; Bothe, E.; Weyhermüller, T.; Wieghardt, K. *J. Am. Chem. Soc.* **2001**, *123*, 6025.
(32) Sokolowski, A.; Adam, B.; Weyhermüller, T.; Kikuchi, A.; Hildenbrand, K.; Schnepf, R.; Hildebrandt, P.; Bill, E.; Wieghardt, K. *Inorg. Chem.* **1997**, *36*, 3702.
(33) Benelli, C.; Dei, A.; Gatteschi, D.; Guedel, H. U.; Pardi, L. *Inorg. Chem.* **1989**, *28*, 3089.

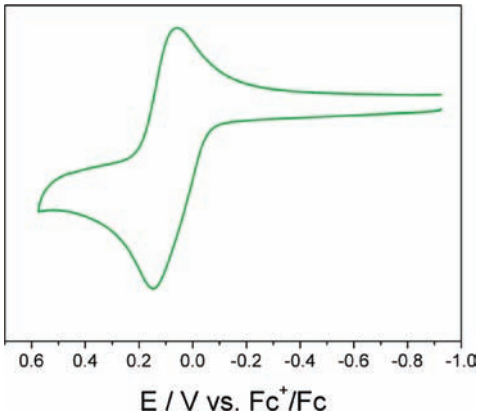


**Figure 7.** Cyclic voltammogram of **2a** in $CH_2Cl_2$ (22 °C, 0.10 M $[N(n\text{-}Bu)_4]PF_6$, scan rate 200 mV $s^{-1}$, glassy carbon working electrode).

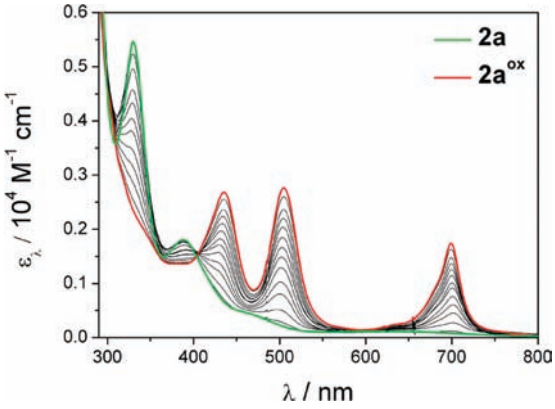


**Figure 8.** Spectral changes in the electronic absorption spectrum upon electrochemical oxidation of **2a** (green) to $\mathbf{2a^{ox}}$ (red) at +400 mV in $CH_2Cl_2$; 0.1 M $[N(n\text{-}Bu)_4]PF_6$, −25 °C.

corresponding chromium complexes[4,5] and to the changes in the cobalt species **1a**.[3] For both cases the oxidation has been assigned as ligand centered. Closer inspection of the recorded spectra shows significant shifts in the isosbestic points, most pronounced in the region around 310 nm. This indicates partial decomposition of the product during the oxidation. In fact, $\mathbf{2a^{ox}}$ is unstable even at −25 °C under an inert atmosphere and decomposes within a few minutes in solution. Therefore, it was not possible to isolate $\mathbf{2a^{ox}}$ as a solid.

**DFT Calculations.** To obtain a better understanding of the electronic structure of the two structurally characterized compounds **1** and **2**, as well as their one-electron oxidized forms $\mathbf{1^{ox}}$ and $\mathbf{2^{ox}}$, DFT calculations were conducted at the B3LYP level. All calculations used spin-unrestricted methods and were performed on complexes containing the unsubstituted $bdt^{2-}$ ligand only. The initial coordinates for the geometry optimizations were taken from the solid state crystal structure of the previously reported complex $[Cr^{III}(tren)(3,6\text{-}DTBsq^{\bullet})]^{2+}$, applying the necessary truncations and modifications. In the initial geometry the five-membered (bdt) chelate adopts a perfectly planar geometry with an angle $\varphi = 0°$. To simplify the discussion of orbital interactions, the molecules were aligned with the *x*-axis bisecting the S−S vector, while the *z*-axis is perpendicular to the S−Cr−S plane. Note that within this internal coordinate system the $d_{xy}$ and the $d_{x^2-y^2}$ orbital are interchanged compared to the standard textbook formalism for

**Table 3.** Comparison of Selected Bond Distances (Å) and Angles (deg) Obtained from DFT Calculations with the Experimental Values

| | **1** (M = Co) | | $\mathbf{1^{ox}}$ | **2** (M = Cr) | | $\mathbf{2^{ox}}$ |
|---|---|---|---|---|---|---|
| | exp. | calc. | calc. | exp. | calc. | calc. |
| M(1)−N(1) | 1.968(2) | 2.006 | 2.009 | 2.1214(18) | 2.156 | 2.144 |
| M(1)−N(2) | 1.989(2) | 2.065 | 2.035 | 2.0919(17) | 2.198 | 2.157 |
| M(1)−N(3) | 1.992(2) | 2.052 | 2.035 | 2.1006(17) | 2.180 | 2.155 |
| M(1)−N(4) | 1.972(2) | 1.996 | 2.014 | 2.0881(17) | 2.145 | 2.150 |
| M(1)−S(1) | 2.2636(7) | 2.291 | 2.304 | 2.3601(6) | 2.368 | 2.398 |
| M(1)−S(2) | 2.2414(7) | 2.248 | 2.268 | 2.3369(6) | 2.301 | 2.347 |
| S(1)−C(1) | 1.760(3) | 1.792 | 1.741 | 1.761(2) | 1.796 | 1.741 |
| S(2)−C(6) | 1.766(2) | 1.786 | 1.730 | 1.773(2) | 1.792 | 1.733 |
| C(1)−C(2) | 1.399(3) | 1.405 | 1.414 | 1.409(3) | 1.404 | 1.414 |
| C(2)−C(3) | 1.389(4) | 1.396 | 1.385 | 1.381(3) | 1.396 | 1.385 |
| C(3)−C(4) | 1.384(4) | 1.401 | 1.425 | 1.392(3) | 1.400 | 1.424 |
| C(4)−C(5) | 1.393(4) | 1.396 | 1.381 | 1.386(3) | 1.396 | 1.382 |
| C(5)−C(6) | 1.400(4) | 1.405 | 1.419 | 1.400(3) | 1.405 | 1.419 |
| C(6)−C(1) | 1.409(3) | 1.407 | 1.443 | 1.404(3) | 1.410 | 1.448 |
| $\varphi$ | 29.19 | 17.28 | 0.63 | 10.45 | 1.52 | 1.03 |

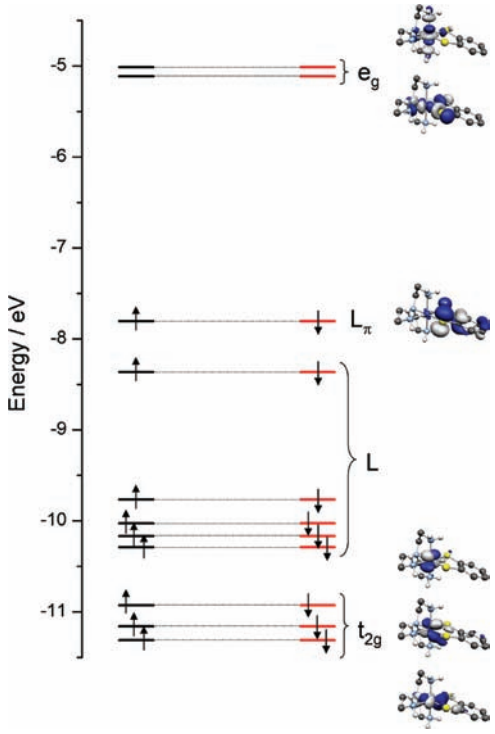


**Figure 9.** MO-scheme for **1** derived from B3LYP DFT calculations.

octahedral complexes. Broken symmetry states, with *n* spin up electrons and *m* spin-down electrons, are denoted by the label BS(*n*,*m*). The broken symmetry approach permits the *n* and *m* electrons to be localized on different areas of the molecule, that is, metal versus ligand, so they can couple magnetically, but are not forcibly paired.

For the diamagnetic cobalt monocation **1** a closed-shell singlet solution ($S = 0$) was found as a stationary state on the potential energy surface. An attempt to calculate a BS (1,1) state corresponding to a ligand radical antiferromagnetically coupled to a low-spin $Co^{II}$ ion, $[Co^{II}(tren)(bdt^{\bullet})]^{+}$, failed; the calculation converged to the closed-shell solution. This is in good agreement with the experimental data from electronic absorption spectroscopy of **1**, which shows no charge transfer bands in the visible region, which would be expected for an open shell

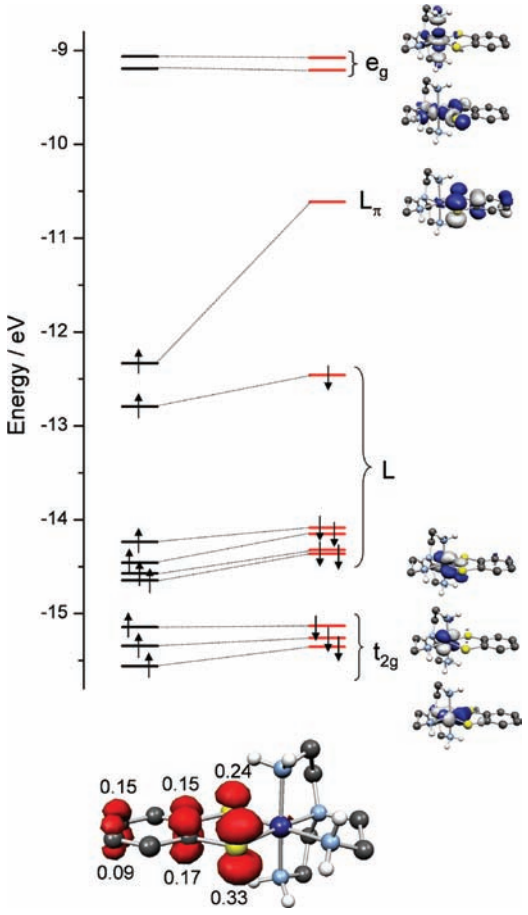


**Figure 10.** Top: MO-scheme for $\mathbf{1}^{ox}$ derived from B3LYP DFT calculations. Bottom: Spin density plot of $\mathbf{1}^{ox}$ obtained from a Mulliken population analysis.

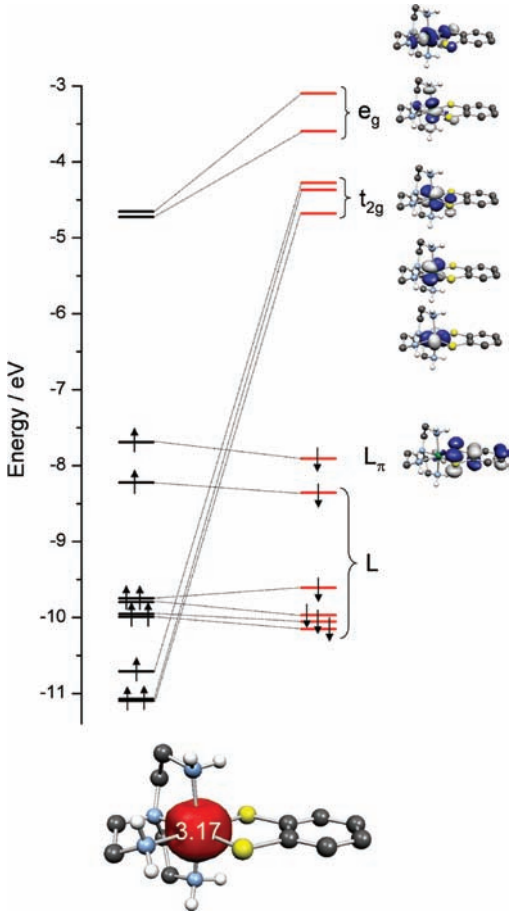


**Figure 11.** Top: MO-scheme for **2** derived from B3LYP DFT calculations. Bottom: Spin density plot of **2** obtained from a Mulliken population analysis.

ligand system. The structural parameters from the geometry optimization, listed in Table 3, are in good agreement with the experimental values. All bond distances in the dithiolene ligand are reproduced within 0.03 Å. The Co−N bond lengths are overestimated by up to 0.08 Å, which is typical for the B3LYP functional.[34]

The molecular orbital (MO) scheme for **1** is shown in Figure 9. Three almost energetically degenerate metal d orbitals are doubly occupied and represent the $t_{2g}$ set in idealized octahedral symmetry. Additionally, two empty d orbitals can be found at higher energy ($e_g$ in octahedral symmetry). This is indicative of a low-spin $Co^{III}$ ion. There are six filled orbitals of the dianionic $bdt^{2-}$ ligand in between these two sets of metal orbitals. Interestingly, the highest unoccupied molecular orbital (HOMO) of the monocation **1** is a ligand $\pi$ orbital with only ~3% cobalt character. Upon oxidation of **1** one electron is removed from this ligand orbital, yielding a $\pi$ radical monoanion *S*,*S*′-coordinated to a $Co^{III}$ ion. The metal d orbital manifold is virtually unchanged (Figure 10). Consequently, the spin density plot derived from a Mulliken population analysis shows that the unpaired electron of the doublet species is spread exclusively over the dithiolene ligand (Figure 10). The calculated structural parameters of $\mathbf{1}^{ox}$ (Table 3) show a quinoidal type distortion of the benzene ring, four long and two short C−C bonds, which is typical for the $\pi$ radical form of dithiolenes. Another important feature is the shortening of the S−C bonds from 1.77 to 1.78 Å down to 1.73−1.74 Å. The calculated folding angle $\varphi$ is very small at 0.63° indicating an almost perfectly planar arrangement of the ligand. This allows for a weak $\pi$ interaction between the half-filled ligand $\pi$ orbital and the $d_{xz}$ orbital on cobalt, which stabilizes the ligand radical. This $\pi$ interaction may also be responsible for the weak hyperfine interactions observed in the EPR spectrum of $\mathbf{1a}^{ox}$.

Calculations for the chromium complex **2** were performed assuming an $S = {}^3/_2$ ground state. The structural parameters are again reproduced with good agreement with the experimental data (±0.03 Å), again with the exception of the metal-to-ligand bonds, which are overestimated by up to 0.1 Å (Table 3). This confirms the formulation as a $Cr^{III}$ complex with a closed shell ligand, which is further supported by the MO-scheme shown in Figure 11. Three half filled ($t_{2g}$) and two empty ($e_g$) Cr d orbitals can be identified establishing the quartet ground state. The ligand remains in its dianionic closed shell form. Figure 11 shows the Mulliken spin density plot for **2**, which confirms that three unpaired electrons are located on the Cr atom, while the ligand is diamagnetic.

In contrast to the calculated structure for the corresponding Co complex **1**, the ligand is arranged in an almost linear fashion ($\varphi$ = 1.52). This may indicate that

(34) Neese, F. *J. Biol. Inorg. Chem.* **2006**, *11*, 702.

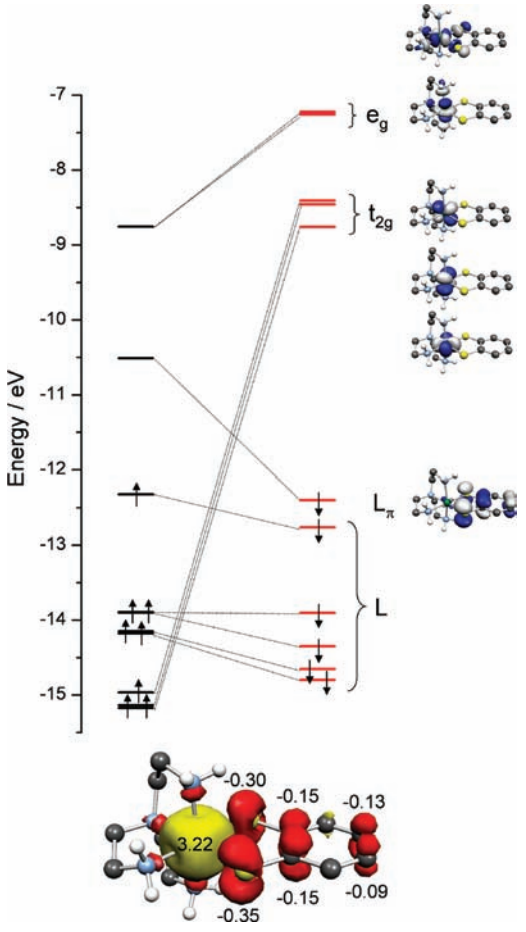


**Figure 12.** Top: MO-scheme for $\mathbf{2^{ox}}$ derived from a BS(3,1) B3LYP DFT calculations. Bottom: Spin density plot (yellow, α-spin; red, β-spin) of $\mathbf{2^{ox}}$ obtained from a Mulliken population analysis.

the $\pi$ interaction between the half-filled $t_{2g}$ set and the ligand is slightly overestimated by DFT. The contribution of Cr to the $L_\pi$ orbital is 8.2%. Although all three singly occupied molecular orbitals (SOMOs) are localized on chromium, they are not the HOMOs of the complex. A closer inspection of the orbital manifold reveals that the $t_{2g}$ set in the α-domain is significantly stabilized. This can only be the result of strong exchange interactions on the $Cr^{III}$ ion. Although less pronounced, this effect also lowers the energy of the $\sigma$ bonding α-orbitals, which possess some metal $e_g$ character. As a result the $\sigma$ bonds between the $e_g$ orbitals and the ligands are spin-polarized, that is, more α-electrons are transferred via covalent interactions to the $Cr^{III}$ center. Therefore, the spin density on the central metal ion exceeds the expectation value of 3.00 in the population analysis. This effect is called spin polarization.

Because of the stabilization of the metal orbitals the HOMO of **2** is a ligand $\pi$ orbital, similar to the case for the cobalt monocation. Accordingly, one electron from this orbital is removed upon oxidation from **2** to $\mathbf{2^{ox}}$. For the oxidized species $\mathbf{2^{ox}}$ a broken symmetry BS(3,1) solution ($S = 1$), corresponding to a $Cr^{III}$ ion with an antiferromagnetically coupled ligand $\pi$ radical, was found as a stable solution on the potential energy surface. Reassuringly, a simple unrestricted triplet state DFT calculation induced spontaneous symmetry breaking and gave an identical solution. Although the spin ground state of $S = 1$ for $\mathbf{2^{ox}}$ could not be verified experimentally because of the low stability of the compound, the calculations showed that the high-spin $S = 2$ state is 5.3 kcal $mol^{-1}$ less favorable. This corresponds to an intramolecular antiferromagnetic coupling constant $J$ of $-1849$ $cm^{-1}$ between the $Cr^{III}$ ion and the dithiolate(1-) $\pi$ radical.

The MO-scheme of $\mathbf{2^{ox}}$ is shown in Figure 12. In comparison with Figure 11 it demonstrates nicely that, as in the cobalt case, the metal orbitals remain almost unchanged after oxidation, while the ligand orbitals are strongly involved in the process.

The optimized structural parameters for the ligand (Table 3) are very similar to those calculated for $[Co^{III}(tren)(bdt^{\bullet})]^{2+}$, $\mathbf{1^{ox}}$, confirming the ligand radical formulation for $\mathbf{2^{ox}}$. The spin density population analysis (Mulliken) summarizes the description as $[Cr^{III}(tren)(bdt^{\bullet})]^{2+}$ for $\mathbf{2^{ox}}$ (Figure 12). Again, the excess of α-spin density on Cr is caused by spin polarization of the $\sigma$-bonds through exchange stabilization of the metal $e_g$ orbitals. Note that the Mulliken spin density on the ligand (1 electron) is located 55% on the two sulfur atoms and only 45% is delocalized onto the phenyl ring. For the corresponding *o*-semiquinonate(1-) ligand in $[Cr^{III}(tren)(sq^{\bullet})]^{2+}$ 70% of the spin density resides on the phenyl ring and only 30% is on the two oxygens. ($sq^{\bullet}$(1-) = 3,6-di-*tert*-butyl-*o*-benzosemiquinonate(1-) and tren = tris(2-aminoethyl)amine).[5]

## Conclusions

The objective of this study has been to generate and spectroscopically characterize stable *S*,*S*′-coordinated benzene-1,2-dithiolate(1-) $\pi$ radical monoanions. This has been achieved by synthesizing octahedral complexes of cobalt(III) (low-spin $d^6$, $S_{Co} = 0$) and chromium(III) ($d^3$, $S = {}^3/_2$) ions bound to a neutral redox-stable tris(2-aminoethyl)amine ligand and a closed-shell benzene-1,2-dithiolate(2-) ligand generating the classic Werner-type monocations $[M^{III}(tren)(benzene\text{-}1,2\text{-}dithiolato)]^+$ (M = Co(III), Cr(III)) where the former possesses a singlet ($S = 0$) and the latter a quartet ($S = {}^3/_2$) ground state. Mulliken spin population analyses of the two species from DFT calculations (B3LYP) reveal that the Co complex possesses no spin density whereas the chromium(III) species has three unpaired electrons in metal-centered d orbitals ($t_{2g}^3$ in $O_h$ symmetry).

Electrochemically both types of complexes can be reversibly one-electron oxidized generating relatively stable dications in $CH_2Cl_2$ solutions. Spectroscopic evidence from their electronic and EPR spectra indicate unambiguously that these one-electron oxidations are ligand centered processes affording the dications $[Co^{III}(tren)(benzene\text{-}1,2\text{-}dithiolate^{\bullet})]^{2+}$ possessing an $S = {}^1/_2$ ground state and $[Cr^{III}(tren)(benzene\text{-}1,2\text{-}dithiolate^{\bullet})]^{2+}$ possessing an $S = 1$ ground state. DFT calculations support this interpretation. Most salient in this respect is the Mulliken spin population of the dicationic cobalt species which shows the presence of a diamagnetic central cobalt(III) ion (low-spin $d^6$, $S_{Co} = 0$) and an *S*,*S*′-coordinated benzene-1,2-dithiolate(1-) $\pi$ radical with one unpaired electron residing in a ligand $\pi$ orbital (SOMO). For the corresponding chromium(III) complex a broken symmetry solution BS(3,1) ($S = 1$) was found, and the

Mulliken spin population clearly indicates the presence of three unpaired electrons in metal d orbitals ($t_{2g}^3$ configuration) and a single unpaired electron in a ligand $\pi$ orbital; these two couple intramolecularly antiferromagnetically yielding an $S = 1$ ground state.

The most important aspect of this analysis pertains to the observed spectroscopic similarities between *O*,*O*′-coordinated *o*-benzosemiquinonate(1-) $\pi$ radicals in $[Co^{III}(trien)(3,5\text{-di-}tert\text{-butylbenzosemiquinonato}^{\bullet})]^{2+}$ in ref 3 and the present *o*-dithiosemiquinonato radical species **1a**$^{ox}$. Similarly, the structurally characterized $[Cr^{III}(tren)(3,6\text{-di-}tert\text{-butylbenzosemiquinonato}^{\bullet})]^{2+}$ and the present dication **2a**$^{ox}$ display very similar electronic spectra.

There appears to be a significant difference in the spin density distribution in the $[Cr^{III}(o\text{-semiquinonato}^{\bullet})]^{2+}$ and $[Cr^{III}(o\text{-dithiosemiquinonato}^{\bullet})]^{2+}$ moieties. While both species display three unpaired electrons at their respective central chromium(III) ions ($t_{2g}^3$), the spin density of the unpaired electron on the ligand resides 70% on the six-membered ring and 30% at the two oxygen atoms in the *o*-benzosemiquinonate complex.[5] In **2**$^{ox}$ this unpaired electron is located 55% on the two sulfur atoms, and only 45% is delocalized onto the phenyl ring.

**Acknowledgment.** We thank Dr. Flavio Benedito for kindly providing the ligand 3,6-bis(trimethylsilyl)benzene-1,2-dithiol. C.M. gratefully acknowledges the Max-Planck Society for a stipend.

**Supporting Information Available:** X-ray crystallographic files in CIF format of **1** and **2**. This material is available free of charge via the Internet at http://pubs.acs.org.